Organic & Biomolecular Chemistry

ROYAL SOCIETY OF CHEMISTRY

PAPER

View Article Online
View Journal | View Issue

Cite this: *Org. Biomol. Chem.*, 2022, **20**, 2889

Design and NMR characterization of reversible head-to-tail boronate-linked macrocyclic nucleic acids†

Mégane Debiais,[a] Alejandro Gimenez Molina,[a] Sabine Müller,[b] Jean-Jacques Vasseur,[a] Ivan Barvik,[c] Carine Baraguey*[a] and Michael Smietana *[a]

Received 2nd February 2022,
Accepted 15th March 2022

DOI: 10.1039/d2ob00232a

rsc.li/obc

Inspired by the ability of boronic acids to bind with compounds containing diol moieties, we envisioned the formation in solution of boronate ester-based macrocycles by the head-to-tail assembly of a nucleosidic precursor that contains both a boronic acid and the natural 2′,3′-diol of ribose. DOSY NMR spectroscopy experiments in water and anhydrous DMF revealed the dynamic assembly of this precursor into dimeric and trimeric macrocycles in a concentration-dependent fashion as well as the reversibility of the self-assembly process. NMR experimental values and quantum mechanics calculations provided further insight into the sugar pucker conformation profile of these macrocycles.

Introduction

Macrocyclic structures are at the heart of intense research activity and are currently expansively investigated in a wide variety of applications in different areas including smart materials, biochemical sensing,[1] ion pair receptors,[2] enantioselective recognition,[3–6] drug delivery[7] and responsive materials.[8,9] The repertoire of supramolecular macrocyclic molecules is vast and encompasses a wide structural variety of which the most known are crown ethers,[10,11] cyclodextrines,[12] rotaxanes and catenanes,[13] cucurbiturils,[14,15] calixarenes,[16,17] pillararenes,[18–20] and resorcinarenes.[21,22] The formation of these macrocyclic structures can be achieved through covalent coupling, dynamic covalent chemistry or noncovalent self-assembly.[8]

Based on the formation of reversible covalent bonds, the synthesis of macrocycles using dynamic covalent chemistry is characterized by its ability to be controlled by changing experimental conditions and external stimuli. The arsenal of reversible reactions is vast and has been described in detail in dedicated recent reviews.[23–27] Among these reactions, boronic acid–diol interactions leading to the formation of stable cyclic boronates have received increasing attention for the elaboration of macrocycles and cages.[28–34]

Traditionally, approaches to form macrocycles *via* boronic ester formation involve to remove water from a mixture composed of a functionalized mono- or di-boronic acid and a polyol.[29,35,36] By contrast, the construction of boronate-based macrocycles using head-to-tail assembly of a molecule carrying both a boronic acid and a diol moiety are rather scarce.[37,38]

Our laboratory has long been interested in the study of DNA-templated formation of reversible boronate internucleoside linkages generated from two strands, one having the natural *cis*-diol functions of ribonucleotides at its 3′-end, while the second one was substituted by a boronic acid at its 5′-extremity.[39–42] Whereas earlier studies relied on the incorporation of 2′-deoxyboronononucleotide phosphoramidites into DNA sequences,[43–45] we recently extended the formation of boronate internucleoside linkages to RNA sequences.[46] This was achieved through the synthesis of a 6′-boronoribonucleotidic 2′-*O*-pivaloyloxymethyl (*O*-PivOM) phosphoramidite building block **2** prepared in 8 steps starting from commercially available 2′-*O*-pivaloyloxymethyl-5′-*O*-dimethoxytrityluridine **1** (Fig. 1A). These results led us to consider the synthesis of a 6′-boronic acid uridine analogue **3** functionalized by both a *cis*-diol moiety and a boronic acid and to evaluate its ability to self-assemble in a head-to-tail (**htt**) fashion to generate boronate-linked macrocyclic nucleotides (Fig. 1B).

Results and discussion

Synthesis of 6′-boronic acid uridine analogue 3

The preparation of compound **3** started from commercially available 2′,3′-*O*-isopropylideneuridine **4** which was oxidized by 2-iodoxybenzoic acid (IBX) in acetonitrile (ACN) to obtain the corresponding 5′-aldehyde **5**. Methylenation of the aldehyde

[a]*Institut des Biomolécules Max Mousseron, Université de Montpellier, CNRS, ENSCM, 1919 route de Mende, 34095 Montpellier, France.*
E-mail: carine.baraguey@umontpellier.fr, michael.smietana@umontpellier.fr
[b]*University Greifswald, Institute for Biochemistry, Greifswald, Germany*
[c]*Institute of Physics, Faculty of Mathematics and Physics, Charles University, Ke Karlovu 5, Prague 2, 121 16, Czech Republic*

†Electronic supplementary information (ESI) available. See https://doi.org/10.1039/d2ob00232a

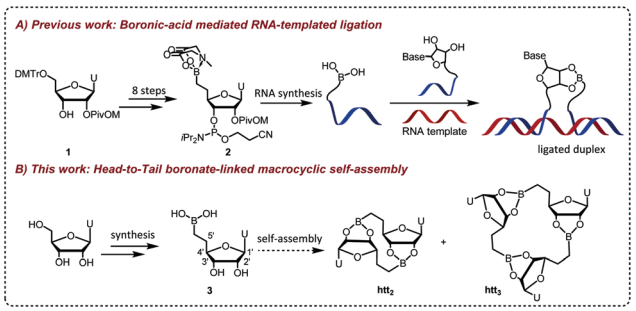

Fig. 1 Schematic illustration of boronic acid-mediated assembly of nucleic acids (DMTr: dimethoxytrityl, U = uracyl).

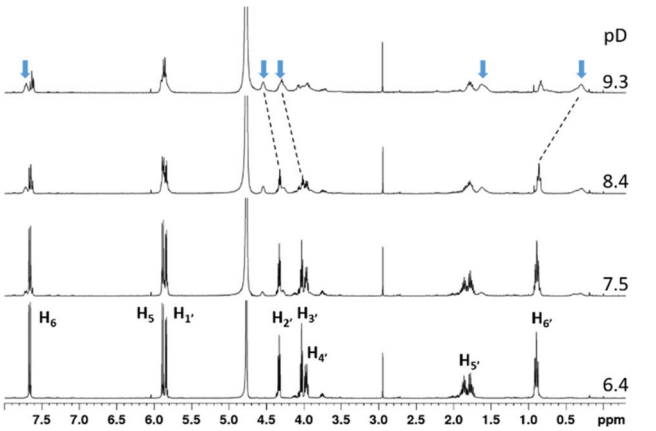

Fig. 2 Effect of pD variations on ^{1}H NMR spectra of compound **3** (37 mM, 298 K). pD values (pD = pH_{read} + 0.4) are reported on the figure. Blue arrows show the peaks that merged under basic conditions. Dotted lines show the shift of $H_{2'}$, $H_{3'}$ and $H_{6'}$ induced by the basicity increase.

group was achieved by means of Nysted reagent to generate 5′-alkene **6**. Removal of the isopropylidene group with trichloroacetic acid (TCA) followed by borylation of the alkene with *in situ* prepared diisopinocampheylborane (IpC_2BH) provided the desired boronic acid **3**. The overall preparation of **3** was thus accomplished in 4 steps and 23% overall yield starting from **4** (Scheme 1).

Characterization of head-to-tail macrocycles

Reversible covalent bonding of boronic acids with diols is well-known to be disfavored in acidic and neutral aqueous media but on the contrary can be promoted under basic conditions.[47] To evaluate if self-assemblies occur in water, a sample of **3** in D_2O (37 mM) was submitted to pD variations by addition of few aliquots of NaOD in D_2O (Fig. 2). Increasing the pD value from 6.4 to 9.3 led to a progressive splitting and broadening of the resonances. New peaks (marked by blue arrows in Fig. 2) merged from pD = 7.5. The one at 0.30 ppm was assigned to 6′-methylene protons. Under basic conditions, the boron is known to coexist under both trigonal and tetragonal forms.[47] Since the methylene in position 6′ is directly bound to boron, the strong high-field shift of $H_{6'}$ was mainly attributed to the change of hybridization of the boron atom from sp^2 to sp^3. As a consequence of the formation of a boronate linkage with $O_{2'}$ and $O_{3'}$ oxygen atoms, two other interesting peaks were noticed at δ = 4.27 and 4.54 ppm which were attributed to $H_{2'}$ and $H_{3'}$ from heteronuclear ^1H–^{13}C spectrum (Fig. S15†).

Decreasing the pD back to 6.4 restored the initial spectrum corresponding to the monomer, thus excluding the observed changes to result from any degradation and demonstrating the reversibility of the process. While these results suggest the reversible self-assembly of **3** in basic aqueous media, detailed insights into the structure were difficult to determine due to the broad spectral features observed.

Compound **3** was thus studied in anhydrous DMF-d_7, a solvent expected to promote the ligation between the boronic acid and the 2′-3′ diol moieties. The ^{1}H NMR spectrum of **3** at 37 mM exhibited two datasets in a 2 : 1 ratio indicating the presence of two species (bottom spectra Fig. 3 and ESI Fig. S13†). Selective saturation experiments (data not shown) confirmed the existence of a slow exchange at the NMR time-scale between the two species since saturation of a signal belonging to the major species affected the corresponding resonance in the minor species.

^{1}H NMR experiments revealed that neither the 2′ and 3′ hydroxyl protons, nor those from the boronic acid function could be observed. Moreover, the boron-bound methylene group at the 6′ position presented a multiplicity more complex than the triplet resulting from the free rotation of the boronic extremity as observed in D_2O. Few aliquots of H_2O were then gradually added to the sample. As expected, this resulted in the disappearance of the two signals around 5.20 and 4.80 ppm assigned to $H_{2'}$ and $H_{3'}$ respectively, that were progressively replaced by two signals at higher field corresponding to the same protons in the free form.

At the same time, three new signals characteristic of the exchangeable hydroxyl protons merged at 5.21, 5.52 and 7.70 ppm (Fig. 3 upper part and Table 1). After addition of 20 μL of water ($4\%_{v/v}$) a unique data set corresponding to the monomer was observed.

Additional ^{1}H NMR spectra were recorded in anhydrous DMF-d_7 for diluted samples, showing the concentration dependence of the two species distribution. Lowering the concentration led to a gradual decrease of the minor species signals. The ratio of the integrations of H_6 peaks for the major

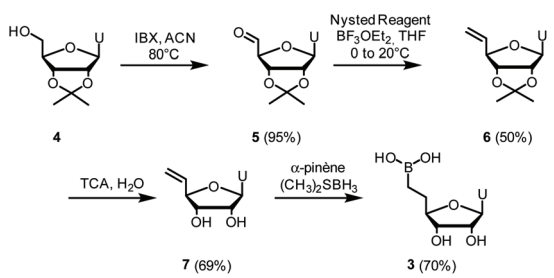

Scheme 1 Chemical synthesis of 6′-boronic acid uridine analogue **3**.

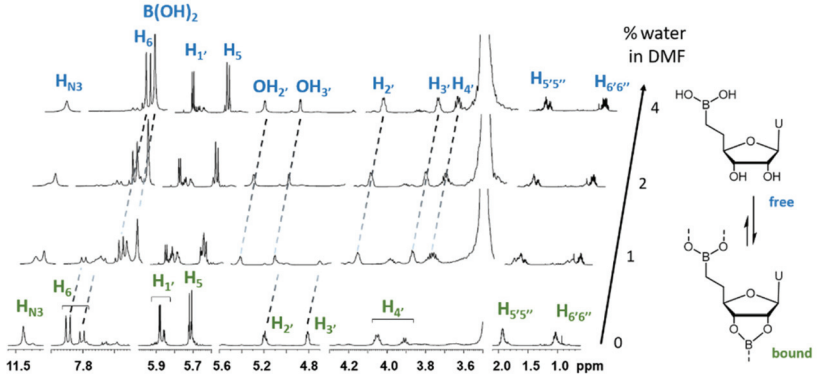

Fig. 3 ^{1}H NMR spectra of **3** in anhydrous DMF-d_7 with increasing quantities of water (for clarity, parts of the spectra free of signal were removed).

Table 1 ^{1}H chemical shifts (ppm) in DMF-d_7

Atom	Anhydrous DMF-d_7		DMF-d_7/H_2O[a] (**3**)	$\Delta\delta$[b]
	Major species[c]	Minor species		
$H_{1'}$	5.88	5.86	5.89	−0.02
$H_{2'}$	5.19	5.18	4.20	+1.02
$H_{3'}$	4.81	4.80	3.92	+0.89
$H_{4'}$	4.05	3.90	3.82	+0.16
$H_{5'/5''}$	1.93	1.91	1.81/1.74	
$H_{6'/6''}$	1.10–0.95	1.10–0.95	0.84/0.78	+0.20
$OH_{2'}$	—	—	5.52	—
$OH_{3'}$	—	—	5.21	—
H_5	5.71	5.72	5.71	+0.01
H_6	7.85	7.81	7.71	+0.12
NH	11.40	11.40	11.33	+0.07
$B(OH)_2$	—	—	7.70	—

[a] H_2O: 4%. [b] Difference (in ppm) between the mean value of the chemical shifts of the 2 species existing in anhydrous DMF-d_7 (water < 0.05%) and the chemical shift of **3** observed in wet DMF-d_7 (water 4%). [c] Major species population estimated to 73% from the H_6 peaks integration and taking into account the di- and trimeric nature of the 2 structures (*vide infra*).

and minor species dropped from 1.7 : 1 at 37 mM to 6.7 : 1 at 1.4 mm. At 0.14 mM, only the major species could be detected. No significant chemical shift change was noticed in this concentration range (0.14 to 37 mM), excluding any self-association due to intermolecular π-stacking interactions (ESI, Fig. S13†).

^{11}B NMR was also investigated and two spectra were acquired under strictly identical conditions for the same sample before and after addition of water (Fig. S12†). The spectrum acquired in DMF-d_7 containing 20 μL of water showed a single and relatively narrow peak at 31.9 ppm characteristic of the free boronic acid with a trigonal geometry around the boron atom. In anhydrous DMF-d_7, a very broad band ranging between 20 and 50 ppm was observed. No significant chemical shift variation could be reported, the signal linewidth in the bound state preventing to detect the chemical shift with accuracy, a characteristic that is well established for ^{11}B atom.[48]

The symmetry loss around the boron center as well as the slower molecular tumbling, both consecutive to the boron-ribose ligation might explain the flattened signal observed in anhydrous DMF. ^{1}H and ^{13}C resonances of the two species coexisting in anhydrous DMF-d_7 were individually assigned and compared to the ones of the monomer **3** generated by addition of water (Tables 1 and 2 and ESI Fig. S14†). Under anhydrous conditions, $H_{2'}$ and $H_{3'}$ protons were both down-field shifted by about 1 ppm (Table 1) compared to the monomer, while the corresponding carbons were shifted by more than 10 ppm (Table 2). Numerous studies on boronic acids complexation with sugars reported that boronate formation leads to a significant down-field shift of both the ^{1}H and ^{13}C resonances of the boron-bound diol moiety in both water and organic solvent.[49,50] Consistent with the literature, these observations showed that the 2′ and 3′ oxygen atoms are bound to boron in both of the two structures coexisting in anhydrous DMF-d_7. The comparison of the signals in anhydrous DMF-d_7 indicated that the two species were structurally close (Tables 1 and 2).

In ^{1}H NMR, the strongest variation between the 2 assemblies was found for $H_{4'}$ (4.05 *vs.* 3.90 ppm, Table 1) while on the ^{13}C spectrum moderate deviations were noticed for the sugar ring atoms, with a maximum variation of 1.3 ppm for $C_{4'}$. The evidence of boronate ester formation with the 2′-3′ *cis*-

Table 2 ^{13}C chemical shifts (ppm) in DMF-d_7

Atom	Anhydrous DMF-d_7		DMF-d_7/H_2O[a] (**3**)	$\Delta\delta$[b]
	Major species	Minor species		
$C_{1'}$	92.4	92.9	88.8	+3.9
$C_{2'}$	84.9	85.3	73.9	+11.2
$C_{3'}$	84.6	83.3	73.5	+10.5
$C_{4'}$	87.4	88.1	86.1	+1.7
$C_{5'}$	27.7	27.3	28.7	−1.2
$C_{6'}$	6.3	6.2	11.3	−5.1
C_2	151.0	150.9	151.2	−0.3
C_4	163.6	163.6	163.6	0
C_5	102.6	102.6	102.2	+0.4
C_6	142.9	143.2	141.2	+1.9

[a] H_2O: 4%. [b] Difference (in ppm) between the mean value of the chemical shifts of the 2 species existing in anhydrous DMF-d_7 (water < 0.05%) and the chemical shift of **3** observed in wet DMF-d_7 (water 4%).

diol moiety and the absence of hydroxyl protons in anhydrous DMF-d_7 suggested the presence of cyclic assemblies rather than linear oligomers.

To determine the size of these structures, diffusion ordered spectroscopy experiments (DOSY) were carried out and confirmed that the 2 sets of signals belonged to different species (Fig. 4). The diffusion coefficient measurements showed that both assemblies diffused at different but still relatively close rates (2.81×10^{-10} m^2 s^{-1} and 3.26×10^{-10} m^2 s^{-1} for the minor and major species respectively, Fig. S20†). The translational diffusion coefficient of the monomeric form was also determined from the sample in wet DMF-d_7 to be 3.84×10^{-10} m^2 s^{-1} (Fig. S21†). Considering that the addition of 4% of water in the sample did not significantly modify the medium viscosity, the diffusion coefficients were used to estimate the molecular weight of each structure using the Stokes–Einstein equation after correction of the *f*-factor according to Gierer and Wirtz (Table 3 and ESI†).[51] From this calculation the molecular weights of the major and minor species were estimated to be 467 and 730 g mol^{-1} respectively. These values were in agreement with calculated molecular weights for dimeric (**htt$_2$**) and trimeric (**htt$_3$**) head-to-tail macrocycles (500 and 750 g mol^{-1} respectively).

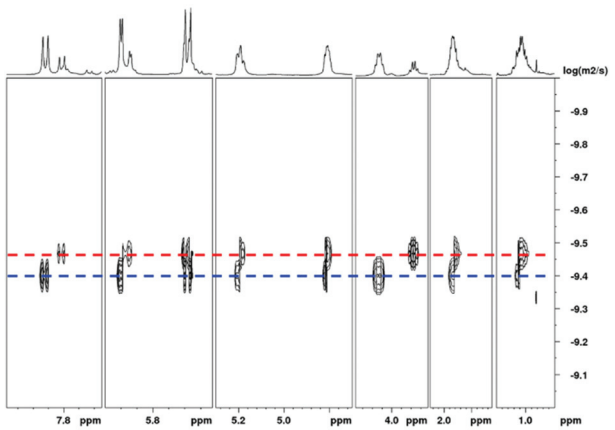

Fig. 4 DOSY spectrum of **3** in anhydrous DMF-d_7 (for clarity purpose, parts of the spectra free of signal were removed). Red and blue dotted lines refer to minor and major species respectively.

To assess the efficiency of the DOSY experiment for the characterization of these dynamic assemblies, we synthesized linear (dinucleotide **U$_2$** and trinucleotide **U$_3$**) and cyclic (**c(T$_2$)** and **c(T$_3$)**) reference compounds and measured their diffusion coefficients in anhydrous DMF-d_7. The linear compounds were prepared using standard automatized phosphoramidite chemistry while the cyclic derivatives were obtained according to the procedure described by Smietana and Kool.[52] The reference compounds were selected for practical reasons assuming that their diffusion coefficients would not differ significantly from **c(U$_2$)** and **c(U$_3$)** which would require more steps to achieve their synthesis. Indeed, an excellent correlation of the diffusion coefficients between the cyclic **c(T$_2$)** and **c(T$_3$)** reference compounds and the corresponding boronate assemblies was obtained (Table 3). Together, these results clearly indicate the head-to-tail formation of boronate-linked macrocyclic nucleotides analogues. Given the rapid opening of these macrocycles in the presence of water, their separation and isolation by HPLC techniques is illusive. We have already demonstrated in the past during DNA-templated ligation experiments that the generated internucleoside boronate linkages were disrupted upon denaturation *i.e.* in the absence of the template.[41,46] The very fact that the boronate-linked macrocycle is formed and observed by NMR in the absence of a matrix is already remarkable.

We then investigated the impact of the boronate linkage on the intrinsic conformational preference of the sugar moiety. First structural insights about the macrocyclic dimer **htt$_2$** were obtained from molecular modeling. The geometry of the structure was optimized by means of quantum mechanics (QM) calculations using the Gaussian 03 software package with the MP2/6-31G(d) method (Fig. 5). Analysis of the sugar ring pucker for this model indicated a flattened $C_{4'\text{-}exo}$ conformation (puckering amplitude Φ_m = 26°). In spite of our efforts we did not succeed in obtaining crystals of **htt$_2$** or **htt$_3$**. Therefore, to experimentally support the molecular modeling results, vicinal coupling constants were analyzed. In free nucleosides, the ribose

Table 3 Diffusion coefficients (in m^2 s^{-1}) measured in dry DMF-d_7 at 298 K[a]

Compound	**3**	**U$_2$**	**U$_3$**	**c(T)$_2$**	**c(T)$_3$**	**htt$_2$**	**htt$_3$**
D ($\times 10^{-10}$ m^2 s^{-1})	3.84	3.19	2.96	3.29	2.86	3.26	2.81

[a] Maximum standard deviation: 0.08×10^{-10} m^2 s^{-1}.

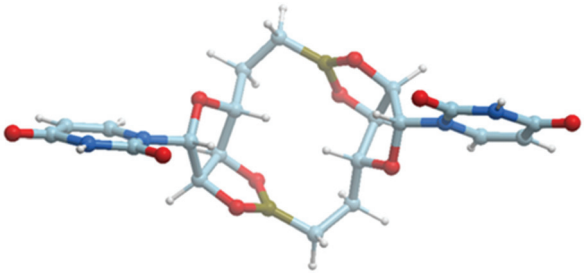

Fig. 5 Structure of **htt$_2$** optimized using QM calculations at the MP2/6-31G(d) level of theory.

adopts a conformation among the most representative forms, namely $C_{2'\text{-}endo}$ (south) and $C_{3'\text{-}endo}$ (north) usually subjected to a rapid interconversion equilibrium.

For the $C_{2'\text{-}endo}$ conformation, typical values of the vicinal coupling constants are found about 8–10 Hz for $^3J_{1'\text{-}2'}$ and 1–2 Hz for $^3J_{3'\text{-}4'}$ while these orders of magnitude are reversed for the $C_{3'\text{-}endo}$ conformation. The three ribose coupling constants for native uridine and its boronic analogue **3** are given in Table S4.† In water, these two compounds presented comparable values, characteristic of mononucleotides operating a dynamic north–south equilibrium. In wet DMF-d_7, the higher $^3J_{1'\text{-}2'}$ value indicated a slight preference of the south conformation. In anhydrous DMF on the contrary, markedly lower $^3J_{1'\text{-}2'}$ constants were observed (3.2 and 2.5 Hz for **htt$_2$** and **htt$_3$** respectively, Table S4†) suggesting a significant prevalence of the north conformation. The population of the north conformers for **3** were estimated to be 53% in water, 47% in wet DMF-d_7 and 68% and 75% in anhydrous DMF-d_7 for **htt$_2$** and **htt$_3$** respectively (calculated from % north = $100 - 10 \times {}^3J_{1'\text{-}2'}$).[54]

On the other hand, $^3J_{2'\text{-}3'}$ coupling constant (~5 Hz in free mononucleotides) is almost unaffected by the north–south equilibrium but strongly depends on the ring pucker.[55,56] For **htt$_2$**, both the rather high $^3J_{2'\text{-}3'}$ value (7.8 Hz) and the lower value of $^3J_{1'\text{-}2'} + {}^3J_{3'\text{-}4'}$ (8.3 Hz compared to 9.5 Hz observed in the classical north–south equilibrium), indicated a flattening of the ribose ring and a possible atypical conformation.

The coupling constants were then calculated from a generalized Karplus equation and empirical relationships between torsion angles and pseudorotation parameters (P and Φ) defined by Altona and coworkers for β-D-ribose,[53] and compared to the experimental values measured for **htt$_2$** (Table 4). The results for ideal $C_{3'\text{-}endo}$ (P = 18°, Φ_m = 37°) and $C_{2'\text{-}endo}$ conformations (P = 162°, Φ_m = 37°) led to predictable markedly high RMS deviations (Table 4, entries 1 and 2). Assuming a single conformation, the phase angle and the ring pucker were then optimized to fit the experimental data (Table 4, entry 3) and P and Φ_m values corresponding to a flattened $C_{4'\text{-}exo}$ conformer, together with a reasonable RMSD (0.21 Hz) were obtained. To evaluate if the coupling constants could result from an equilibrium between flattened $C_{2'\text{-}endo}$ and $C_{3'\text{-}endo}$ conformations, the calculations were then repeated assuming a symmetrical two states model (*e.g.* $\Phi_N = \Phi_S$) and optimizing both the molar fraction of the $C_{3'\text{-}endo}$ conformer (X_N) and the Φ values. In this case, calculated values were found to fit the experimental data with a reasonable deviation (0.14 Hz) when reducing the pucker amplitude to 15° and for a population of the north conformer of 70% (Table 4, entry 4). Finally, a last calculation was run assuming an equilibrium between the $C_{4'\text{-}exo}$ conformation and any other south conformer, optimizing P_N, Φ_m and X_N values (Table 4, entry 5). In that case, the best RMSD deviations was reached (0.03 Hz) for a $C_{4'\text{-}exo} \leftrightarrow C_{4'\text{-}endo}$ type equilibrium, with a population of 69% of the $C_{4'\text{-}exo}$ form.

Both the single conformation (Table 3, entry 3) and the north ↔ south equilibrium models (Table 4, entries 4 and 5) gave reliable fitting results, although in the former case the calculations led to an overestimation of the vicinal $^3J_{2'\text{-}3'}$ constant (0.3 Hz).

To determinate whether the sugar maintains a certain flexibility or is conformationally locked, the coupling constants temperature-dependence was assessed. ^{1}H NMR spectra were recorded at 273 K and 333 K and almost unchanged J values were measured (ΔJ_{max} = 0.2 Hz). This confirmed that the sugar was frozen in a rigid $C_{4'\text{-}exo}$ conformation as highlighted by the molecular modeling study. Nucleosides bridged at the 2′ and 3′ position either by an alkyl chain[57] or by a phosphate group have been already reported in the literature.[58,59] In solution, 2′-3′-*O*-methoxymethyluridine was reported as a flexible system engaged in a $C_{2'\text{-}endo} \leftrightarrow C_{3'\text{-}endo}$ equilibrium with a slightly flattened pucker (Φ_m = 34°)[57] and 2′-3′-phosphate cyclic mononucleosides were considered as similar flexible systems.[58] By contrast 2′-3′-isopropylidene nucleosides were described as rigid structures.[60]

Table 4 Calculated coupling constants for **htt$_2$**

Entry	Model	P_N [a] (°)	Φ_N [a] (°)	P_S [a] (°)	Φ_S [a] (°)	X_N [b]	$J_{1'\text{-}2'}$ [c] (Hz)	$J_{2'\text{-}3'}$ [c] (Hz)	$J_{3'\text{-}4'}$ [c] (Hz)	RMSD[d] (Hz)
1	$C_{3'\text{-}endo}$	18	37				1.20	5.14	8.79	2.87
2	$C_{2'\text{-}endo}$			162	37		7.85	5.20	1.24	3.80
3	Single conformer	52	9				3.13	8.15	5.12	0.21
4	$C_{2'\text{-}endo} \leftrightarrow C_{3'\text{-}endo}$	18	15	162	15	0.70	3.06	7.66	4.97	0.14
5	$C_{4'\text{-}exo} \leftrightarrow C_{4'\text{-}endo}$	54	20	234	20	0.69	3.17	7.85	5.11	0.03

[a] P and Φ are the amplitude puckering and the phase angle of pseudorotation respectively, as defined by Haasnoot *et al.*[53] [b] X_N represents the mole fraction of the north conformer. [c] Experimental values obtained for **htt$_2$**: $^3J_{1'\text{-}2'}$ = 3.2 Hz; $^3J_{2'\text{-}3'}$ = 7.8 Hz; $^3J_{3'\text{-}4'}$ = 5.1 Hz. [d] RMSD = root-mean-square deviation.

Whenever the structures were studied in liquid or in solid state, the formation of a fused five-membered ring bridging the 2′ and 3′ oxygen atoms clearly constrains the ribose, thus severely reducing the pucker amplitude (Φ_m between 17 and 32°) compared to that commonly found in unmodified nucleosides and nucleotides (Φ_m about 39°).[61] The macrocycle described here presented an additional constraint due to the 5′-2′/3′ head-to-tail cyclization that probably contribute to the structure rigidity.

Comparison of the dihedral exocyclic angles from QM geometry optimization and for the 2 models resulting from the fitting of the NMR data are given in Table S5.† Both NMR and QM gave comparable angles values, characteristic of a favored north $C_{4'\text{-}exo}$ conformation with a reduced pucker amplitude thus corroborating the formation of the cyclic homodimer **htt$_2$**.

Several nucleoside derivatives adopting a favored $C_{4'\text{-}exo}$ conformations have already been reported in the literature. In all cases, these derivatives are constrained either by chemical modifications of the sugar,[62–64] or because of an association of a nucleotide with a protein target.[65]

The 6′-boronic acid uridine analogue **3** described here is an example of a highly constrained structure, due to both the formation of a five-membered-ring at the 2′-3′ extremities of the sugar and the head-to-tail cyclization.

Conclusion

Boronic acids are attractive building blocks that are being increasingly used for the construction of organized architectures. While the vast majority of boronate-based macrocycles and cages are constructed by the dynamic assembly of a functionalized mono- or di-boronic acid with a polyol, we present here the formation of an original type of macrocycles based on boronate esters resulting from the head-to-tail self-assembly of a nucleoside carrying both a boronic acid and a *cis*-diol moiety. These results set the stage for investigating the formation of macrocycles from a mixture of pyrimidines and purine 5′-boronic acid analogues. While we have already reported the synthesis of the whole set of 5′-boronic acid 2′-deoxy-nucleotide analogues,[44] we are currently working on the preparation of these analogues in the RNA series.

Author contributions

M. D.: investigation, methodology, visualization, validation. A. G. M.: investigation, methodology, resources. S. M.: funding acquisition, project administration, supervision, writing–review and editing. J. J. V.: methodology, writing–review and editing. I. B.: formal analysis, investigation, resources. C. B. conceptualization, formal analysis, investigation, supervision, writing – original draft. M. S.: conceptualization, funding acquisition, project administration, supervision, writing – original draft.

Conflicts of interest

There are no conflicts to declare.

Acknowledgements

The Agence Nationale de la Recherche and the Deutsche Forschungsgemeinschaft are gratefully acknowledged for financial support (ANR PCRI "TEMPLAR"-16-CE92-0010-01; DFG MU1396/11). The research leading to these results has also received funding from the People Programme (Marie Curie Actions) of the European Union's Seventh Framework Programme (FP7/2007–2013) under REA grant agreement n. PCOFUND-GA-2013-609102, through the PRESTIGE programme coordinated by Campus France.

Notes and references

1 R. Pinalli, A. Pedrini and E. Dalcanale, *Chem. Soc. Rev.*, 2018, **47**, 7006–7026.
2 Q. He, G. I. Vargas-Zúñiga, S. H. Kim, S. K. Kim and J. L. Sessler, *Chem. Rev.*, 2019, **119**, 9753–9835.
3 P. D. Frischmann and M. J. MacLachlan, *Chem. Soc. Rev.*, 2013, **42**, 871–890.
4 V. N. Khose, M. E. John, A. D. Pandey, V. Borovkov and A. V. Karnik, *Symmetry*, 2018, **10**, 34.
5 R. Ning, H. Zhou, S. X. Nie, Y. F. Ao, D. X. Wang and Q. Q. Wang, *Angew. Chem., Int. Ed.*, 2020, **59**, 10894–10898.
6 D. Kauerhof and J. Niemeyer, *ChemPlusChem*, 2020, **85**, 889–899.
7 D. Y. Xia, P. Wang, X. F. Ji, N. M. Khashab, J. L. Sessler and F. H. Huang, *Chem. Rev.*, 2020, **120**, 6070–6123.
8 J. Yu, D. Qi and J. Li, *Commun. Chem.*, 2020, **3**, 189.
9 X. P. Yang, H. J. Yu, L. Wang, R. B. Tong, M. Akram, Y. S. Chen and X. T. Zhai, *Soft Matter*, 2015, **11**, 1242–1252.
10 S. Di Stefano, G. Capocasa and L. Mandolini, *Eur. J. Org. Chem.*, 2020, 3340–3350.
11 B. Zheng, F. Wang, S. Y. Dong and F. H. Huang, *Chem. Soc. Rev.*, 2012, **41**, 1621–1636.
12 W. J. Xu, X. M. Li, L. Wang, S. Y. Li, S. N. Chu, J. C. Wang, Y. J. Li, J. X. Hou, Q. A. Luo and J. Q. Liu, *Front. Chem.*, 2021, **9**, 635507.
13 M. J. Langton and P. D. Beer, *Acc. Chem. Res.*, 2014, **47**, 1935–1949.
14 Y. H. Liu, Y. M. Zhang, H. J. Yu and Y. Liu, *Angew. Chem., Int. Ed.*, 2021, **60**, 3870–3880.
15 E. Pazos, P. Novo, C. Peinador, A. E. Kaifer and M. D. Garcia, *Angew. Chem., Int. Ed.*, 2019, **58**, 403–416.
16 Y. C. Pan, X. Y. Hu and D. S. Guo, *Angew. Chem., Int. Ed.*, 2021, **60**, 2768–2794.
17 R. Kumar, A. Sharma, H. Singh, P. Suating, H. S. Kim, K. Sunwoo, I. Shim, B. C. Gibb and J. S. Kim, *Chem. Rev.*, 2019, **119**, 9657–9721.

18 T. Ogoshi, T. Kakuta and T. Yamagishi, *Angew. Chem., Int. Ed.*, 2019, **58**, 2197–2206.
19 Y. Y. Fang, Y. Deng and W. Dehaen, *Coord. Chem. Rev.*, 2020, **415**, 213313.
20 Q. Li, H. T. Z. Zhu and F. H. Huang, *Trends Chem.*, 2020, **2**, 850–864.
21 C. Gaeta, C. Talotta, M. De Rosa, P. La Manna, A. Soriente and P. Neri, *Chem. – Eur. J.*, 2019, **25**, 4899–4913.
22 N. Natarajan, E. Brenner, D. Semeril, D. Matt and J. Harrowfield, *Eur. J. Org. Chem.*, 2017, 6100–6113.
23 A. Herrmann, *Chem. Soc. Rev.*, 2014, **43**, 1899–1933.
24 S. P. Black, J. K. M. Sanders and A. R. Stefankiewicz, *Chem. Soc. Rev.*, 2014, **43**, 1861–1872.
25 R. C. Brachvogel and M. von Delius, *Eur. J. Org. Chem.*, 2016, 3662–3670.
26 Y. H. Jin, C. Yu, R. J. Denman and W. Zhang, *Chem. Soc. Rev.*, 2013, **42**, 6634–6654.
27 Y. H. Jin, Q. Wang, P. Taynton and W. Zhang, *Acc. Chem. Res.*, 2014, **47**, 1575–1586.
28 R. Nishiyabu, Y. Kubo, T. D. James and J. S. Fossey, *Chem. Commun.*, 2011, **47**, 1124–1150.
29 N. Christinat, R. Scopelliti and K. Severin, *Angew. Chem., Int. Ed.*, 2008, **47**, 1848–1852.
30 N. Christinat, R. Scopelliti and K. Severin, *Chem. Commun.*, 2008, 3660–3662.
31 B. J. Smith, N. Hwang, A. D. Chavez, J. L. Novotney and W. R. Dichtel, *Chem. Commun.*, 2015, **51**, 7532–7535.
32 H. Takata, K. Ono and N. Iwasawa, *Chem. Commun.*, 2020, **56**, 5613–5616.
33 A. D. Chavez, B. J. Smith, M. K. Smith, P. A. Beaucage, B. H. Northrop and W. R. Dichtel, *Chem. Mater.*, 2016, **28**, 4884–4888.
34 J. Liu and J. J. Lavigne, in *Boronic Acids*, Wiley-VCH, 2011, pp. 621–676.
35 N. Iwasawa and H. Takahagi, *J. Am. Chem. Soc.*, 2007, **129**, 7754–7755.
36 D. G. Hall, *Boronic acids*, Wiley-VCH, 2011.
37 B. K. Shull, D. E. Spielvogel, R. Gopalaswamy, S. Sankar, P. D. Boyle, G. Head and K. Devito, *J. Chem. Soc., Perkin Trans. 2*, 2000, 557–561.
38 S. Chirayil and K. J. Luebke, *Tetrahedron Lett.*, 2012, **53**, 726–729.
39 A. R. Martin, I. Barvik, D. Luvino, M. Smietana and J.-J. Vasseur, *Angew. Chem., Int. Ed.*, 2011, **50**, 4193–4196.
40 R. Barbeyron, J.-J. Vasseur and M. Smietana, *Chem. Sci.*, 2015, **6**, 542–547.
41 R. Barbeyron, A. R. Martin, J.-J. Vasseur and M. Smietana, *RSC Adv.*, 2015, **5**, 105587–105591.
42 G. Clavé, M. Reverte, J.-J. Vasseur and M. Smietana, *RSC Chem. Biol.*, 2021, **2**, 94–150.
43 D. Luvino, C. Baraguey, M. Smietana and J. J. Vasseur, *Chem. Commun.*, 2008, **44**, 2352–2354.
44 A. R. Martin, K. Mohanan, D. Luvino, N. Floquet, C. Baraguey, M. Smietana and J. J. Vasseur, *Org. Biomol. Chem.*, 2009, **7**, 4369–4377.
45 M. Debiais, A. Lelievre, J.-J. Vasseur, S. Müller and M. Smietana, *Chem. – Eur. J.*, 2021, **27**, 1138–1144.
46 A. Gimenez Molina, I. Barvik, S. Müller, J.-J. Vasseur and M. Smietana, *Org. Biomol. Chem.*, 2018, **16**, 8824–8830.
47 G. Springsteen and B. Wang, *Tetrahedron*, 2002, **58**, 5291–5300.
48 H. Nöth and B. Wrackmeyer, *Nuclear Magnetic Resonance Spectroscopy of Boron Compounds*, Springer-Verlag, Berlin, New York, 1978.
49 J. C. Norrild and H. Eggert, *J. Am. Chem. Soc.*, 1995, **117**, 1479–1484.
50 H. Someya, T. Itoh and S. Aoki, *Molecules*, 2017, **22**, 1650.
51 A. Gierer and K. Wirtz, *Z. Naturforsch., A: Astrophys., Phys. Phys. Chem.*, 1953, **8**, 532–538.
52 M. Smietana and E. T. Kool, *Angew. Chem., Int. Ed.*, 2002, **41**, 3704–3707.
53 C. A. G. Haasnoot, F. A. A. M. de Leeuw, H. P. M. de Leeuw and C. Altona, *Org. Magn. Reson.*, 1981, **15**, 43–52.
54 C. Altona and M. Sundaralingam, *J. Am. Chem. Soc.*, 1973, **95**, 2333–2344.
55 C. Altona and M. Sundaralingam, *J. Am. Chem. Soc.*, 1972, **94**, 8205–8212.
56 J. P. Marino, H. Schwalbe and C. Griesinger, *Acc. Chem. Res.*, 1999, **32**, 614–623.
57 A. J. de Kok, C. Romers, H. P. M. de Leeuw, C. Altona and J. H. van Boom, *J. Chem. Soc., Perkin Trans. 2*, 1977, 487–493.
58 C. F. G. C. Geraldes and R. J. P. Williams, *Eur. J. Biochem.*, 1978, **85**, 471–478.
59 D. B. Davies and H. Sadikot, *J. Chem. Soc., Perkin Trans. 2*, 1983, 1251–1258.
60 C. Thibaudeau, J. Plavec and J. Chattopadhyaya, *J. Am. Chem. Soc.*, 1994, **116**, 8033–8037.
61 W. Saenger, *Principles of nucleic acid structure*, Springer Science & Business Media, 1984.
62 P. S. Pallan, V. E. Marquez and M. Egli, *Biochemistry*, 2012, **51**, 2639–2641.
63 P. Rungta, M. Kumar, P. Mangla, S. Kumar and A. K. Prasad, *New J. Chem.*, 2021, **45**, 1609–1616.
64 R. R. Nikam, S. Harikrishna and K. R. Gore, *Eur. J. Org. Chem.*, 2021, 924–932.
65 P. R. Rosevear, V. M. Powers, D. Dowhan, A. S. Mildvan and G. L. Kenyon, *Biochemistry*, 1987, **26**, 5338–5344.